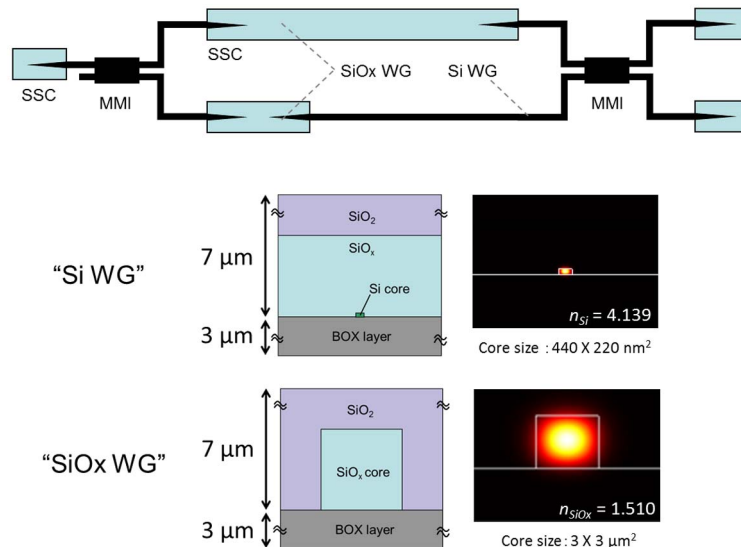


# Silicon/Silica-Hybrid-Integrated Delay Line Interferometer for Demodulation of PSK Formats

Volume 5, Number 2, April 2013

Rai Kou, Member, IEEE  
Hiroshi Fukuda, Member, IEEE  
Tai Tsuchizawa  
Hidetaka Nishi  
Tatsurou Hiraki  
Koji Yamada, Member, IEEE

*Silicon/silica-hybrid-integrated DLI*



---

DOI: 10.1109/JPHOT.2013.2258145  
1943-0655/\$31.00 ©2013 IEEE

# Silicon/Silica-Hybrid-Integrated Delay Line Interferometer for Demodulation of PSK Formats

Rai Kou,<sup>1,2</sup> Member, IEEE, Hiroshi Fukuda,<sup>1,2</sup> Member, IEEE, Tai Tsuchizawa,<sup>1,2</sup>  
Hidetaka Nishi,<sup>1,2</sup> Tatsuro Hiraki,<sup>1,2</sup> and Koji Yamada,<sup>1,2</sup> Member, IEEE

<sup>1</sup>NTT Microsystem Integration Laboratories, NTT Corporation, 3-1,  
Morinosato Wakamiya, Atsugi, Kanagawa 243-0198, Japan

<sup>2</sup>Nanophotonics Center, NTT Corporation, 3-1, Morinosato Wakamiya,  
Atsugi, Kanagawa 243-0198, Japan

DOI: 10.1109/JPHOT.2013.2258145  
1943-0655/\$31.00 ©2013 IEEE

Manuscript received March 18, 2013; revised April 10, 2013; accepted April 10, 2013. Date of publication April 15, 2013; date of current version April 19, 2013. Corresponding author: R. Kou (e-mail: takahashi.rai@lab.ntt.co.jp).

**Abstract:** We propose a 1-bit delay line interferometer (DLI) with a hybrid Mach–Zehnder structure for demodulation of phase-shift-keying (PSK) signals. Each arm contains silicon (Si)/Si-rich silica waveguides and spot size converters to generate optical delay using both of physical length and refractive index changes. This report covers the numerical analysis and experimental investigations, ranging from basic characterization to application. We employed a DLI with a free spectral range of 10.2 GHz in a demodulation experiment of 10.0-Gb/s NRZ-DPSK signals. As a result, very clear eye patterns and error-free operation are obtained from the C- to L-telecommunications bands with a device size per channel of 1.6 mm<sup>2</sup>. The novel and effective design provides a demodulator in simple and high-density device integration.

**Index Terms:** Silicon (Si) photonics, integrated circuits, delay line interferometer (DLI), phase demodulation.

## 1. Introduction

Silicon (Si) photonics technologies are attracting interest not only for optical networks, in applications ranging from optical interconnection to telecommunications, but also for quantum optics [1], bio/environment sensors [2], and other applications. We have developed Si photonics technologies to adapt them to future middle- and short-reach telecommunications networks, where major breakthroughs are required in order to accomplish compact, low cost, scalable, and integrable photonic devices. A CMOS-compatible optically and electrically integrated Si photonic circuit well meets the requirements. The coming generation (in 3 ~ 5 years) of short-reach optical networks will begin to adopt a mixture of WDM and TDM formats [3], and we have actually demonstrated a one-chip monolithically integrated 16-ch WDM receiver [4], [5]. Later in the coming generation (in 5 ~ 10 years), we expect that various advanced modulation formats, such as multilevel phase shift keying (M-PSK) [6], [7], multilevel quadrature amplitude modulation (M-QAM) [8], and orthogonal frequency division multiplexing (OFDM) [9], would be suitable, because they promise great improvements of bandwidth utilization efficiency and the optical signal-to-noise ratio (OSNR) in comparison with the traditional on-off-keying (OOK) formats. These kinds of signals can be detected in two ways: coherent detection or direct differential detection (or differentially coherent detection in [10]). Coherent detection systems are costly and consume high electric power because

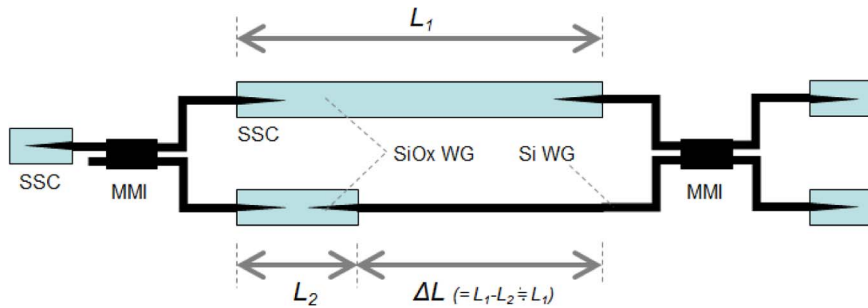


Fig. 1. Schematic of Si/SiOx-hybrid structure.  $L_1$  and  $L_2$  correspond to each waveguide length of SiOx.

they need a digital signal processor (DSP) and local oscillator (LO) to compensate for various signal degradations. On the other hand, direct differential detection with delay line interferometers (DLIs) is a very reasonable solution, especially for middle- and short-reach networks. Previously reported DLIs have mostly been constructed from free-space optics with a Michelson interferometer [11] and a low- $\Delta$  silica planar lightwave circuit (PLC) or optical fibers with a Mach–Zehnder interferometer [12]–[15]. Recently, two types of unique PSK demodulators have been demonstrated using Si photonics technologies: a dual-bus microring resonator working as an extremely narrow frequency discriminator [16], [17] and high-aspect-ratio single Si waveguide working as a 1-bit polarization DLI [18]. Here, we propose a new PSK demodulator constructed with a hybrid Mach–Zehnder structure using Si and Si-rich silica (SiOx) [5] materials. This unique device enables a simple, compact, and high-quality demodulator, which can be additionally arranged in a simple layout when compared with previous just physically delayed 1-bit DLIs: all of them are constructed on the basis of controlling the propagation length between the two arms. We proposed this basic idea in [19], and in this paper, we develop it to fully understand the fundamental and advanced characteristics of the device, covering a numerical extinction ratio (ER) analysis, the detailed device layout, and measurements of temperature dependence, bit-error rate (BER) characteristics, and laser frequency offset dependence. Recently, we found a new paper that describes an unbalanced MZI with a 2-D Si photonic crystal and simple Si wire waveguide loaded in each arm [20]. The fundamental idea may be similar, but the device is focused on applications of nonlinear switching and wavelength conversion, so that the contents of characterizations are nonlinear effect observations.

In the following section, we start with the numerical estimation and simulation for the proposed PSK demodulator. Then, we show the measured basic and advanced characteristics of a fabricated device.

## 2. Device Design, Analysis, and Fabrication

A schematic of the designed Si/SiOx DLI is shown in Fig. 1. The spot size converters (SSCs) [21] are installed to suppress the coupling losses at the input/output surface and connect between Si and SiOx waveguides in each arm. A  $2 \times 2$ -port MMI is provided to obtain differential signal with balanced photodiodes (PDs) at the output. The total delay for the DLI made of the hybrid structure can be expressed as

$$\{n_{g,SiOx}L_2 + n_{g,si}(L_1 - L_2)\} - n_{g,SiOx}L_1 = c \cdot \Delta T \quad (1)$$

where  $n_{g,si}$  and  $n_{g,SiOx}$  are the group refractive indices of Si and SiOx waveguides,  $L_1$  and  $L_2$  are the SiOx waveguide lengths for each arm,  $c$  is the speed of light in vacuum, and  $\Delta T$  is a 1-bit slot of the modulation rate.

We start the calculation of the propagation mode profiles using a fully vectorial 2-D mode solver in FIMMWAVE [22]. The dimensions of each waveguide are as follows: The core widths for Si and SiOx are 440 nm and 3  $\mu$ m, and the core thicknesses are 220 nm and 3  $\mu$ m. The buried oxide thickness of the SOI wafer is 3  $\mu$ m. Fig. 2(a) shows the profiles, where the group refractive indices are 4.139 for the Si waveguide ( $n_{g,si}$ ) and 1.510 for the SiOx one ( $n_{g,SiOx}$ ). Consequently, the

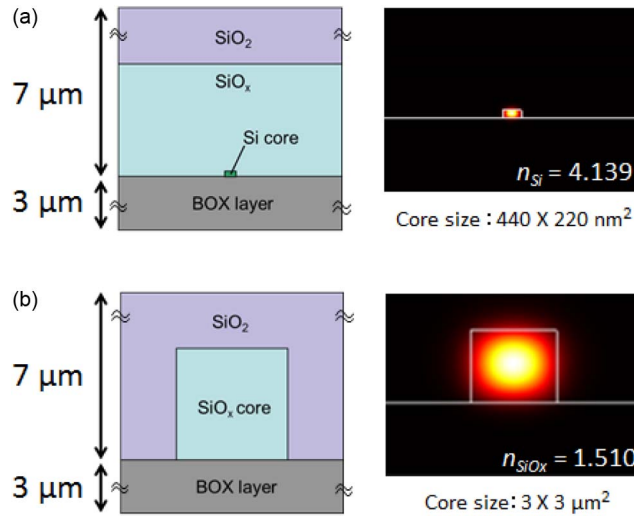


Fig. 2. Calculated mode profiles of (a) Si and (b) SiO<sub>x</sub> waveguides with dimensions of 440 nm × 220 nm and 3 μm × 3 μm, respectively.

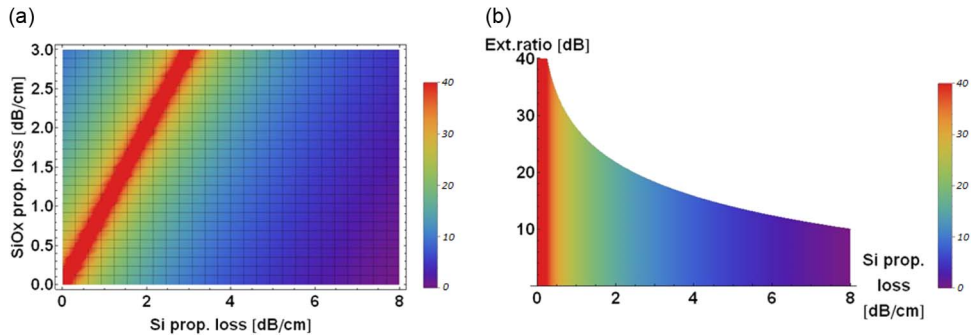


Fig. 3. Numerical estimations of ER for (a) Si/SiO<sub>x</sub>-hybrid DLI and (b) conventional Si DLI.

required waveguide length for 10.0-Gb/s demodulation is estimated to be approximately 1.140 cm from (1). Assuming various fluctuations induced from the group refractive index calculation and fabrication process, we set as parameters nine length differences between SiO<sub>x</sub> waveguides in the upper arm and lower arm  $L_1 - L_2 = \Delta L$ : 1.040, 1.065, 1.090, 1.115, 1.140, 1.165, 1.190, 1.215, and 1.240 cm.

Taking the hybrid structure with different lengths and different propagation losses into consideration, we estimated the ER of the Si/SiO<sub>x</sub>-hybrid DLI, which can be calculated from the following expression:

$$\text{Ext. ratio} = 20 \cdot \log_{10} \left[ \frac{\{10^{(L_{\text{SiO}_x, \text{upper}} \cdot P_{\text{SiO}_x} / 10)}\}^{1/2} - \{10^{((L_{\text{SiO}_x, \text{lower}} \cdot P_{\text{SiO}_x} + L_{\text{Si}, \text{lower}} \cdot P_{\text{Si}}) / 10)}\}^{1/2}}{\{10^{(L_{\text{SiO}_x, \text{upper}} \cdot P_{\text{SiO}_x} / 10)}\}^{1/2} + \{10^{((L_{\text{SiO}_x, \text{lower}} \cdot P_{\text{SiO}_x} + L_{\text{Si}, \text{lower}} \cdot P_{\text{Si}}) / 10)}\}^{1/2}} \right] \quad (2)$$

where  $L_{\text{SiO}_x, \text{upper/lower}}$  and  $L_{\text{Si}, \text{lower}}$  are the waveguide lengths of the Si and SiO<sub>x</sub> waveguides (*upper* or *lower* corresponds to each MZI arm), and  $P_{\text{SiO}_x}$  and  $P_{\text{Si}}$  are the propagation losses of the Si and SiO<sub>x</sub> waveguides. Fig. 3 shows 2-D mapping of numerically estimated ER for the (a) Si/SiO<sub>x</sub>-hybrid DLI and a (b) conventional Si DLI, respectively. From these results, while the ER in the conventional Si DLI is fixed by propagation loss of the Si waveguide, the Si/SiO<sub>x</sub>-hybrid DLI has flexibility to control propagation loss of Si or SiO<sub>x</sub>. Especially for Si waveguides, in which it is not easy to achieve negligibly low propagation loss, there are no methods to obtain the desired ER. To control

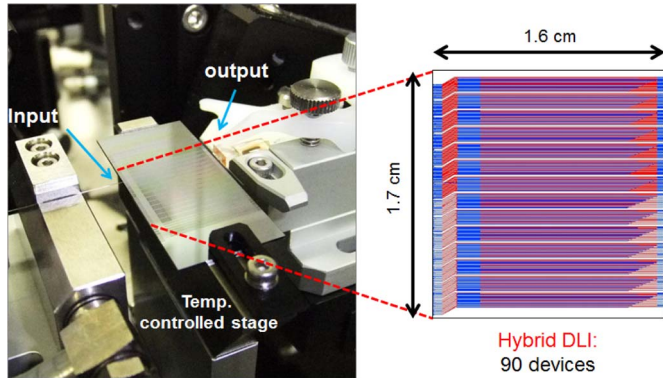


Fig. 4. Photograph of the experiment setup and device CAD layout.

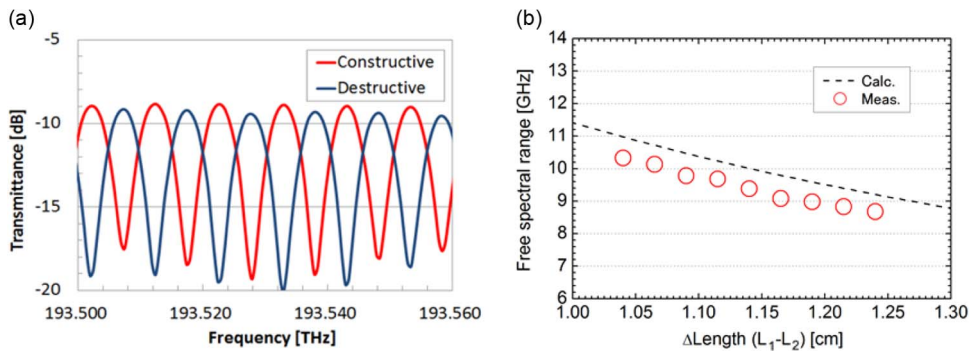


Fig. 5. (a) Interference spectra of constructive and destructive ports around the wavelength of 1550 nm (193.5 THz). Observed FSR is 10.2 GHz; ER is  $\sim 10$  dB. (b) Comparison between calculated and measured FSRs, which are functions of device length difference  $\Delta L$  at wavelength of 1550 nm.

the loss, we have developed an approach for SiOxNy, in which the loss is caused by strong resonance absorption due to the overtone of the O–H and N–H stretching vibration. The absorption efficiency (also refractive index) can be widely controlled by changing O<sub>2</sub> and N<sub>2</sub> flows in the film deposition process. The details are described in [23]. This is another advantage of constructing a hybrid structure. The point of view can also be applied to change or compensate for temperature or dispersion dependence in MZI.

In the fabrication process, the Si waveguides and SSCs with an inverse taper structure [21] were defined by electron beam lithography and electron cyclotron resonance (ECR)–reactive ion etching (RIE) on conventional 4-in SOI wafer. Next, SiO<sub>2</sub> and SiOx were deposited by ECR–chemical vapor deposition (CVD), and the structure was defined by RIE. The refractive index of SiOx is controlled by changing the O<sub>2</sub> flow rate. The fabrication process is described in more detail in [24] and [5]. The total size of each DLI is approximately 1.6 mm<sup>2</sup> (16 mm  $\times$  0.1 mm), which includes separation gaps on both sides.

### 3. Basic Device Characterization

We first measured the optical losses of Si and SiOx waveguides as basic device characterizations. A C-band amplified spontaneous emission (ASE) light source was used to couple the input/output SSCs with high-NA optical fibers of a 4.1- $\mu$ m mode-field diameter. The propagation losses of Si and SiOx for TE mode were measured as 5.0 and 1.1 dB/cm, respectively, and coupling losses for input/output ports of SiOx were measured as 0.6 dB/facet. Fig. 4 shows a photograph of the measurement setup and a schematic of the device layout, where 90 hybrid DLIs are integrated in an area of 1.7 cm  $\times$  1.6 cm. Fig. 5(a) shows the transmitted interference spectra of constructive and

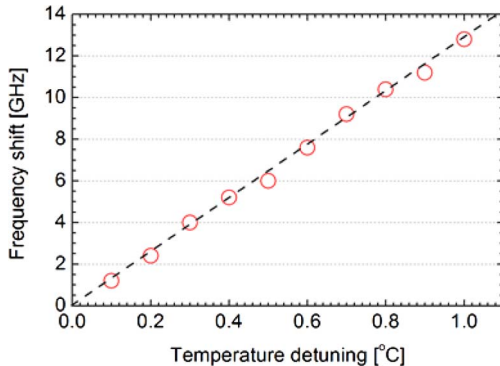


Fig. 6. Frequency shift dependence of temperature detuning with a DLI of  $\Delta L$ : 1.065 cm.

destructive ports for length difference  $\Delta L$  of a 1.065-cm-long hybrid DLI around the wavelength of 1550 nm ( $\sim 193.5$  THz), measured with an optical spectrum analyzer (OSA). A free spectrum range (FSR) of 10.2 GHz and an ER of  $\sim 10$  dB are obtained, respectively. The reason for degradation of the ER is slightly higher propagation loss of the Si waveguides as mentioned above, which induces imbalance interference. A numerical estimation showed that, with an improvement to 2 dB/cm, an ER of over 25 dB can be obtained as shown in Fig. 3(a). Fig. 5(b) compares calculated and measured FSRs, which are functions of length difference  $\Delta L$  at 1550 nm. The slight difference in the FSRs between the calculation and experiment could be due to structural errors in the fabrication process.

Toward future practical use in systems, the temperature sensitivity and controllability should be investigated for this interferometer. Thermal shifts generally come from the thermo-optic (TO) effect in Si and SiO<sub>x</sub> materials (SiO<sub>x</sub> can be assumed as SiO<sub>2</sub>). However, even though the coefficients ( $\Delta n / \Delta T$ ) are well known as  $1.9 \times 10^{-4} 1/\text{°C}$  [25] and  $1.2 \times 10^{-5} 1/\text{°C}$  [26], the actual TO effect is not easy to estimate compared with weakly confined waveguides. This is because in highly confined waveguides, especially in a Si waveguide in this case, it strongly depends on the materials' structure and the mode profile. We therefore used a DLI with  $\Delta L$  of 1.065 cm to identify the dependence of the frequency shift on temperature detuning with a digital controlled heater. This length was chosen because, as described in the next section, the demodulation experiment was performed at 10.0 Gb/s, and it is equivalent to the bit rate. Fig. 6 shows measurement plots with a linear fitting line, where the coefficient of 12.8 GHz/°C (from 29 to 30 °C) was measured at 1550 nm. The value corresponds approximately to one fifth compared with that of bulk silicon materials.

#### 4. DPSK Demodulation

Many complex modulation formats, such as DQPSK, are based on binary modulation signals, so we chose the simplest format, DPSK, to characterize the demodulation performance. A schematic of the setup for the DPSK modulation and demodulation are shown in Fig. 7. We used a C-/L-band tunable laser diode (TLD), a pulse pattern generator (PPG), and a zero-chirp LiNbO<sub>3</sub> Mach-Zehnder modulator, biased at null for phase modulation, to generate a nonreturn-to-zero (NRZ) 10.0-Gb/s pseudorandom bit stream (PRBS) with length of  $2^{31} - 1$ . We employed a DLI with  $\Delta L$  of 1.065 cm, which has FSR of 10.2 GHz. The polarization state of the input light was adjusted to the TE mode with a polarization controller. A high-NA optical fiber of a 4.1-μm mode-field diameter was used for coupling at the input surface, and a multichannel 50-μm-pitch fiber array block formed by etching the top cladding region of high-NA fibers was used for coupling at the output surface. The special narrow-pitch array block is designed to reduce separating fields for each channel, which has significant effects on total size, especially on large-scale integrated and packaged devices. Before the time-based signal quality characterizations, we observed demodulated spectra at the output ports with the OSA. Ideal constructive and destructive spectra [6] are shown in Fig. 8(a) and (b). Subsequently, the demodulated output signal was fed into commercially available balanced

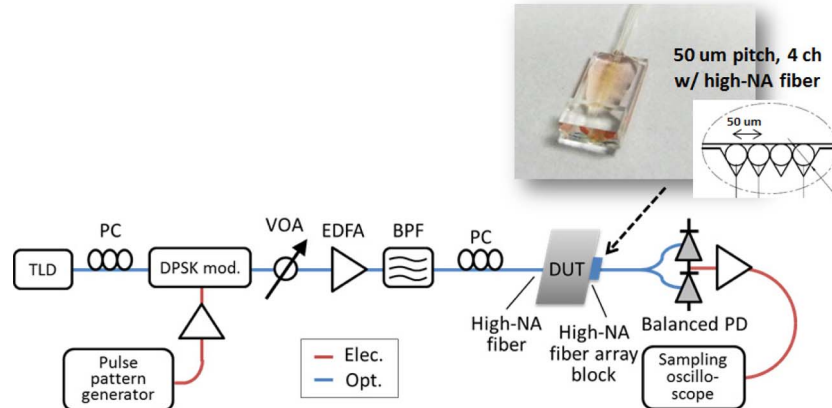


Fig. 7. Schematic of the setup for signal pattern observation and BER measurements of DPSK signal. Photograph of a multichannel 50- $\mu\text{m}$ -pitch fiber array block is shown at the top-right of the figure.

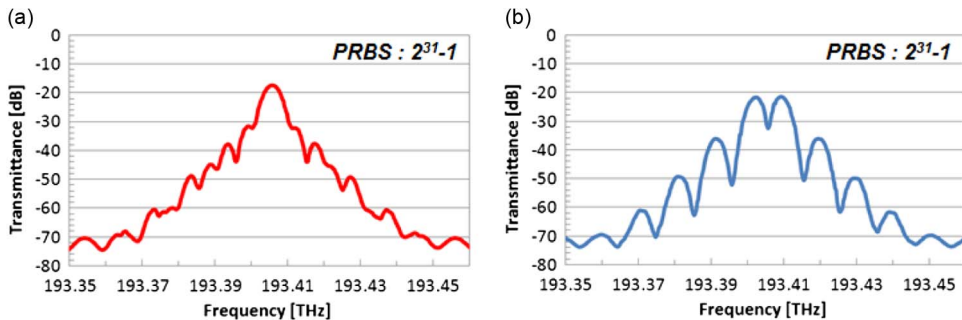


Fig. 8. Demodulated spectra from (a) constructive and (b) destructive ports at 1550 nm observed with the OSA. All spectra were obtained with a modulation bit rate of 10.0 Gb/s and PRBS length of 2<sup>31</sup> – 1.

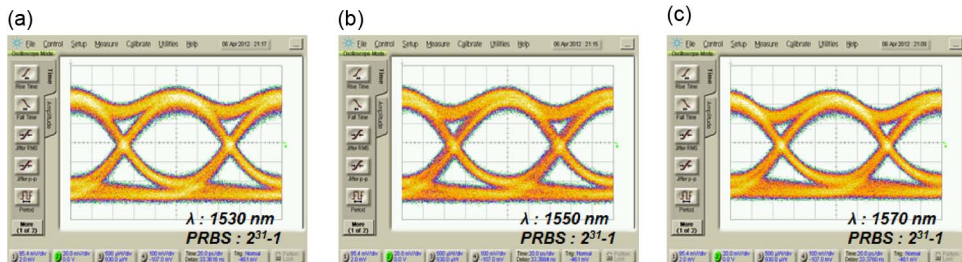


Fig. 9. Demodulated eye diagrams at (a) 1530, (b) 1550, and (c) 1570 nm. All eye patterns were obtained with a modulation bit rate of 10.0 Gb/s and PRBS length of 2<sup>31</sup> – 1.

PDs simultaneously to maximize the detection sensitivity with the DPSK format. It is characterized with a sampling digital oscilloscope. Fig. 9(a)–(c) shows 10.0-Gb/s eye diagrams of demodulated signals. Clear eye openings are obtained at wavelengths of 1530, 1550, and 1570 nm.

Next, we positioned several optical components and an error detector for BER measurements. As shown in Fig. 10(a), error-free operation was determined by measuring up to a BER of 10<sup>-9</sup> at a bit rate 10.0 Gb/s with PRBS length of 2<sup>31</sup> – 1. The minimum detection power at BER of < 10<sup>-12</sup> was estimated to be around –25 dBm. We also confirmed the power requirements for BER of 10<sup>-9</sup> versus laser frequency offset of the TLD. As shown in Fig. 10(b), for 1-dB power penalty, the tolerance is 1.8 GHz (–1.0 ~ +0.8 GHz), which corresponds that the device has acceptance for

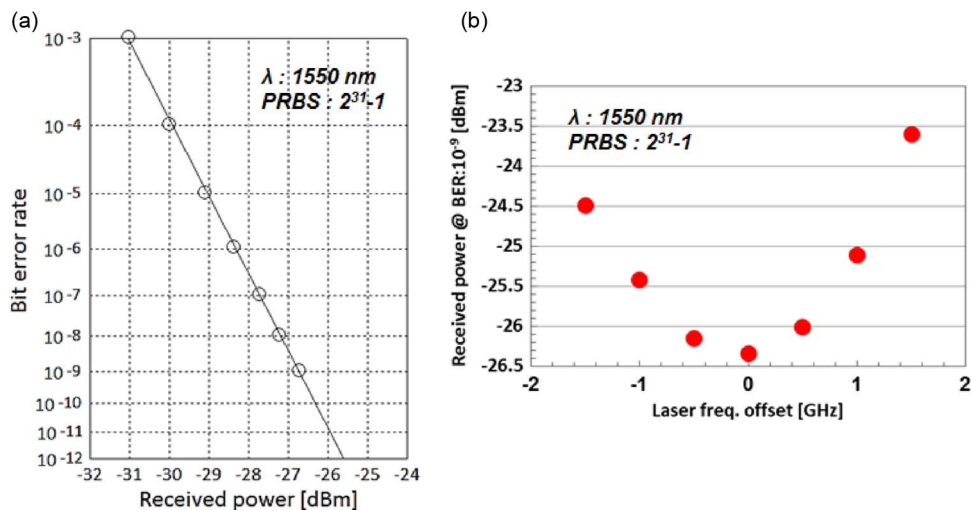


Fig. 10. (a) BER measurement. (b) Power requirements for  $\text{BER} = 1 \times 10^{-9}$  versus laser frequency offset in the TLD. All results were obtained with a modulation bit rate of 10.0 Gb/s and PRBS length of  $2^{31} - 1$ .

maximum temperature variation of  $\sim 0.15^\circ\text{C}$  (cf. temperature dependence measurement in Fig. 6). Note that the performance specifications of the commercial thermal electric cooler are sufficient for the value.

One concern about these kinds of extremely compact demodulators based on Si and related materials are that they basically work only with one polarization mode. The problem especially appears in telecommunications applications, which require polarization-independent devices. Well-designed waveguide dimensions and structures could compensate for the polarization mode dispersion and polarization dependent loss simultaneously, but this is really hard to achieve and would result in lost design flexibility. Fortunately, we have demonstrated directional-coupler-based polarization rotators and polarization beam splitters based on an offset-axis dual core waveguide with broadband operations [27]–[29], which can be integrated on a Si platform. This means a polarization-diversity configuration is utilizable for this DLI.

In addition, one of our future concepts for PSK demodulation applications is to integrate epitaxially grown germanium PDs and trans-impedance amplifiers with compact Si/SiO<sub>x</sub>-based optical devices, such as WDM receivers demonstrated in [4].

## 5. Conclusion

We have proposed a Mach–Zehnder DLI based on a hybrid Si/SiO<sub>x</sub> structure, which can be applied to various applications such as a PSK demodulator and optical interleaver. The isometric and simple DLI design will contribute to the development to large-scale Si photonics integration. In this paper, we have first focused on the concept, design, and basic optical characterizations of the DLI. Then, we have demonstrated 10.0-Gb/s NRZ-DPSK demodulation in a fabricated device. Taken together, the experiment results and signal-quality measurements indicate excellent performance. The proposed device would therefore be one possible choice for the PSK demodulator in short- and middle-reach telecommunications networks for the next generation.

## Acknowledgment

The authors thank T. Watanabe and Dr. S. Itabashi of NTT Advanced Technology for CAD design and device fabrication, K. Konishi of Waseda University for device design and simulation assistance, T. Goh of NTT Photonics Laboratories for BER measurement and helpful discussions. They also thank Dr. S. Mino of NTT Photonics Laboratories for encouragement.

## References

- [1] H. Takesue, Y. Tokura, H. Fukuda, T. Tsuchizawa, T. Watanabe, K. Yamada, and S. Itabashi, "Entanglement generation using silicon wire waveguide," *Appl. Phys. Lett.*, vol. 91, no. 20, pp. 201108-1–201108-3, Nov. 2007.
- [2] X. Xu, A. Densmore, A. Delage, P. Waldron, R. McKinnon, S. Janz, J. Lapointe, G. Lopinski, T. Mischki, E. Post, P. Cheben, and H. Schmid, "Folded cavity SOI microring sensors for high sensitivity and real time measurement of biomolecular binding," *Opt. Exp.*, vol. 16, no. 19, pp. 15 137–15 148, Sep. 2008.
- [3] J. Kani, "Enabling technologies for future scalable and flexible WDM-PON and WDM/TDM-PON Systems," *IEEE J. Sel. Topics Quantum Electron.*, vol. 16, no. 5, pp. 1290–1297, Sep./Oct. 2010.
- [4] H. Nishi, T. Tsuchizawa, R. Kou, H. Shinojima, T. Yamada, H. Kimura, Y. Ishikawa, K. Wada, and K. Yamada, "Monolithic integration of a silica AWG and Ge photodiodes on Si photonic platform for one-chip WDM receiver," *Opt. Exp.*, vol. 20, no. 8, pp. 9312–9321, Apr. 2012.
- [5] T. Tsuchizawa, K. Yamada, T. Watanabe, S. Park, H. Nishi, R. Kou, H. Shinojima, and S. Itabashi, "Monolithic integration of silicon-, germanium-, and silica-based optical devices for telecommunications applications," *IEEE J. Sel. Topics Quantum Electron.*, vol. 17, no. 3, pp. 516–525, May/Jun. 2011.
- [6] A. H. Gnauck and P. J. Winzer, "Optical phase-shift-keyed transmission," *J. Lightw. Technol.*, vol. 23, no. 1, pp. 115–130, Jan. 2005.
- [7] P. J. Winzer and R. J. Essiambre, "Advanced modulation formats for high-capacity optical transport networks," *J. Lightw. Technol.*, vol. 24, no. 12, pp. 4711–4728, Dec. 2006.
- [8] M. Nakazawa, S. Okamoto, T. Omiya, K. Kasai, and M. Yoshida, "256-QAM (64 Gb/s) coherent optical transmission over 160 km with an optical bandwidth of 5.4 GHz," *IEEE Photon. Technol. Lett.*, vol. 22, no. 3, pp. 185–187, Feb. 2010.
- [9] S. L. Jansen, I. Morita, T. C. W. Schenck, N. Takeda, and H. Tanaka, "Coherent optical 25.8-Gb/s OFDM transmission over 4160-km SSMAF," *J. Lightw. Technol.*, vol. 26, no. 1, pp. 6–15, Jan. 2008.
- [10] E. Ip, A. P. T. Lau, D. J. F. Barros, and J. M. Kahn, "Coherent detection in optical fiber systems," *Opt. Exp.*, vol. 16, no. 2, pp. 753–791, Jan. 2008.
- [11] X. Liu, A. H. Gnauck, X. Wei, J. Hsieh, C. Y. Ai, and V. Chien, "Athermal optical demodulator for OC-768 DPSK and RZ-DPSK signals," *IEEE Photon. Technol. Lett.*, vol. 17, no. 12, pp. 2610–2612, Dec. 2005.
- [12] Y. K. Lize, M. Faucher, E. Jarry, P. Ouellette, E. Villeneuve, A. Wetter, and F. Seguin, "Phase-tunable low-loss, S-, C-, and L-band DPSK and DQPSK demodulator," *IEEE Photon. Technol. Lett.*, vol. 19, no. 23, pp. 1886–1888, Dec. 2007.
- [13] J. Gamet and G. Pandraud, "C- and L-band planar delay interferometer for DPSK decoders," *IEEE Photon. Technol. Lett.*, vol. 17, no. 6, pp. 1217–1219, Jun. 2005.
- [14] Y. Nasu, K. Hattori, T. Saida, Y. Hashizume, and Y. Sakamaki, "Silica-based adaptive-delay DPSK demodulator with a cascaded Mach-Zehnder interferometer configuration," in *Proc. ECOC*, 2010, pp. 1–3.
- [15] Y. Sakamaki, Y. Nasu, T. Hashimoto, K. Hattori, Y. Inoue, and H. Takahashi, "Silica waveguide DQPSK demodulator with wide operation range enhanced by using stress release grooves," *IEEE Photonics Technol. Lett.*, vol. 21, no. 13, pp. 938–940, Jul. 2009.
- [16] L. Zhang, J. Y. Yang, M. Song, Y. Li, B. Zhang, R. G. Beausoleil, and A. E. Willner, "Microring-based modulation and demodulation of DPSK signal," *Opt. Exp.*, vol. 15, no. 18, pp. 11 564–11 569, Sep. 2007.
- [17] R. Kou, S. Park, T. Tsuchizawa, H. Fukuda, H. Nishi, H. Shinojima, and K. Yamada, "Phase demodulation of DPSK signals using dual-bus coupled silicon micro-ring resonator," *IEICE Trans. Electron.*, vol. E95-C, no. 2, pp. 224–228, 2012.
- [18] R. Kou, H. Nishi, T. Tsuchizawa, H. Fukuda, H. Shinojima, and K. Yamada, "Single silicon wire waveguide based delay line interferometer for DPSK demodulation," *Opt. Exp.*, vol. 20, no. 10, pp. 11 037–11 045, May 2012.
- [19] R. Kou, H. Fukuda, T. Tsuchizawa, H. Nishi, T. Hiraki, and K. Yamada, "Silicon/silica-hybrid delay line interferometer for DPSK demodulation," in *Proc. IEEE 9th Int. Conf. GFP*, 2012, pp. 174–176.
- [20] I. Glesk, P. J. Bock, P. Cheben, J. H. Schmid, J. Lapointe, and S. Janz, "All-optical switching using nonlinear subwavelength Mach-Zehnder on silicon," *Opt. Exp.*, vol. 19, no. 15, pp. 14 031–14 039, Jul. 2011.
- [21] T. Shoji, T. Tsuchizawa, T. Watanabe, K. Yamada, and H. Morita, "Low loss mode size converter from 0.3  $\mu\text{m}$  square Si wire waveguides to singlemode fibres," *Electron. Lett.*, vol. 38, no. 25, pp. 1669–1670, Dec. 2002.
- [22] A. Sv Sudbo, "Film mode matching: A versatile numerical method for vector mode field calculations in dielectric waveguides," *J. Opt. A, Pure Appl. Opt.*, vol. 2, no. 3, pp. 211–233, May 1993.
- [23] K. Yamada, T. Tsuchizawa, H. Fukuda, C. Koos, J. Pfeifle, J. H. Schmid, P. Cheben, P. J. Bock, and A. P. Knights, "Guided light in silicon-based materials," in *Handbook of Silicon Photonics, Series in Optics and Optoelectronics*. Boca Raton, FL, USA: CRC Press, 2013.
- [24] T. Tsuchizawa, K. Yamada, H. Fukuda, T. Watanabe, J. Takahashi, M. Takahashi, T. Shoji, E. Tamechika, S. Itabashi, and H. Morita, "Microphotonics devices based on silicon microfabrication technology," *IEEE J. Sel. Topics Quantum Electron.*, vol. 11, no. 1, pp. 232–240, Jan./Feb. 2005.
- [25] G. Cocorullo, F. G. Della Corte, and I. Rendina, "Temperature dependence of the thermo-optic coefficient in crystalline silicon between room temperature and 550 K at the wavelength of 1523 nm," *Appl. Phys. Lett.*, vol. 74, no. 22, pp. 3338–3340, May 1999.
- [26] J. H. Wray and J. T. Neu, "Refractive index of several glasses as a function of wavelength and temperature," *J. Opt. Soc. Amer.*, vol. 59, no. 6, pp. 774–776, Jun. 1969.
- [27] H. Fukuda, K. Yamada, T. Tsuchizawa, T. Watanabe, H. Shinojima, and S.-I. Itabashi, "Ultrasmall polarization splitter based on silicon wire waveguides," *Opt. Exp.*, vol. 14, no. 25, pp. 12 401–12 408, Dec. 2006.
- [28] H. Fukuda, K. Yamada, T. Tsuchizawa, T. Watanabe, H. Shinojima, and S.-I. Itabashi, "Polarization rotator based on silicon wire waveguides," *Opt. Exp.*, vol. 16, no. 4, pp. 2628–2635, Feb. 2008.
- [29] H. Fukuda, K. Yamada, T. Tsuchizawa, T. Watanabe, H. Shinojima, and S.-I. Itabashi, "Silicon photonic circuit with polarization diversity," *Opt. Exp.*, vol. 16, no. 7, pp. 4872–4880, Mar. 2008.